Human Head Exposure to Bluetooth Frequency - Thermal Response

H. Dodig*, K. Vidjak†, M. Škiljo‡, D. Poljak§
* Faculty of Maritime Studies, University of Split, Split, Croatia
hdodig@pfst.hr
† Faculty of Electrical Engineering, Mechanical Engineering and Naval Architecture, University of Split, Split, Croatia
Klementina.Vidjak.00@fesb.hr
‡ Faculty of Electrical Engineering, Mechanical Engineering and Naval Architecture, University of Split, Split, Croatia
msekelja@fesb.hr
§ Faculty of Electrical Engineering, Mechanical Engineering and Naval Architecture, University of Split, Split, Croatia
dpoljak@fesb.hr

***Abstract*—This paper presents the computation of the steady-state thermal response of the IEEE-recommended computational phantom due to time-harmonic electromagnetic fields at bluetooth frequencies. The computation consists of three steps: solving the inhomogeneous electromagnetic (EM) scattering problem to obtain the electric field distribution, computing the specific absorption rate (SAR), and solving Pennes' bioheat equation. The inhomogeneous EM scattering problem is addressed using a hybrid boundary element/finite element method (BEM/FEM) with edge elements—a computationally expensive approach. However, this study demonstrates that significant reduction in computational cost can be achieved by carefully crafting the computational model. Once the electric field distribution is known, it serves as a volumetric heat source in Pennes' bioheat equation, which is then solved using FEM. As expected from EM theory, the results indicate that at bluetooth frequencies, EM heating is predominantly localized at the surface of the phantom.**

***Index Terms*—Inhomogeneous EM scattering, SAR computation, bio-heat equation, thermal rise, EM dosimetry.**

I. Introduction

THE established biological effect of EM fields in the bluetooth frequency range $2.402\,\mathrm{GHz}$ - $2.480\,\mathrm{GHz}$ is tissue heating [1], [2] and related specific absorption rate (SAR) quantifies how much electromagnetic (EM) energy is absorbed per unit mass of the tissue. Given that the human head contains critical organs such as brain, eyes and ears it is of particular importance to asses the effect of EM fields on these biological structures.

Direct measurements of the temperature increase and SAR in the human head are very difficult, making computational methods and related phantoms an indispensable tools in EM exposure assessment. These methods simulate EM fields within biological tissues, allowing researchers to accurately estimate SAR and predict thermal effects. Numerical methods such as the finite-difference time-domain (FDTD), finite element method (FEM), boundary element method (BEM), methods of moments (MoM) solve Maxwell's equations enabling us to compute the related SAR and the temperature increase.

The calculation of steady-state temperature increase in the human head caused by EM fields is in fact a three step process. The first step involves solving time-harmonic electromagnetic scattering problem for inhomogeneous targets (human head) using one of established methods being either hybrid MoM/FEM [3], [4] or hybrid BEM/FEM with edge elements [5], [6] in order to obtain the electric field distribution inside and at the surface of the human head.

The second step involves the computation of SAR in the human head tissues based on the electric field values obtained in previous step. The final step is to solve Pennes bio-heat differential equation involving EM sources calculated from SAR values. This step is usually carried using FEM as a computational technique.

Hence, this paper is divided into four main sections: in the first section we describe the FEM/BEM method based on edge elements for solving the inhomogeneous EM scattering problem. The second section provides details and explain intricacies of the computational model used in our calculations. The third section focuses on SAR computation while fourth section presents the calculation of steady state thermal response of the human head to EM wave at bluetooth frequencies.

II. Electric field Calculation - Inhomogeneous EM Scattering Problem

As explained in the introduction, the first step in the calculation of thermal response to bluetooth frequency EM fields is calculation of the electric field values inside the computational domain shown in the Fig. 1. The excitation is time harmonic plane wave at frequency $f = 2.45\,\mathrm{GHz}$ with power density $100\,\mathrm{mW/m^2}$.

This work was supported by the Croatian Science Foundation under the project number HRZZ-IPS-2024-02-7779.

979-8-3315-4472-0/25/$31.00 ©2025 IEEE

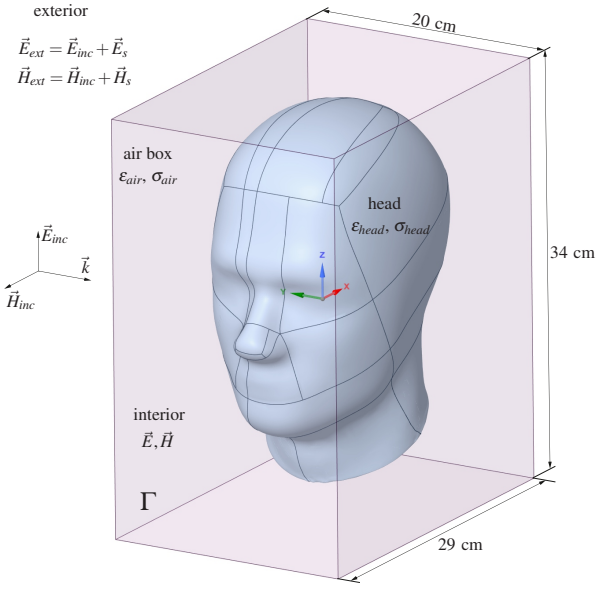

Fig. 1. The plane wave is incident on the inhomogeneous computational domain of size $29\,\mathrm{cm} \times 20\,\mathrm{cm} \times 34\,\mathrm{cm}$ consisting of head and air enclosure (air box). The plane wave of frequency $f = 2.45\,\mathrm{GHz}$ and power density $100\,\mathrm{mW/m^2}$ is impinging on the air box from the left.

The problem with solving inhomogeneous EM scattering problem shown in the Fig. 1 comes from imposing the boundary conditions on the bounding surface Γ of the computational problem. The scattered field must be allowed to propagate to infinity otherwise the artificial reflections from the boundary of the computational domain (surface of airbox) may occur. These artificial reflections can be remedied using perfectly matched layers (PML's) [8] or absorbing boundary conditions (ABC's) [9], [10].

While PML's and ABC's are useful computational techniques, the mathematically correct way to treat the scattered field is by using BEM or MoM. With BEM, the total exterior magnetic field (outside airbox) can be represented by the Stratton-Chu surface integral equation [7]:

$$\begin{aligned}\alpha\vec{H}_{ext} =& \vec{H}_{inc} + \oint_\Gamma \nabla' G \left(\vec{H}_{ext} \cdot d\vec{S}'\right) + \\ & j\omega\epsilon \oint_\Gamma d\vec{S}' \times G\vec{E}_{ext} + \oint_\Gamma \left(d\vec{S}' \times \vec{H}_{ext}\right) \times \nabla' G\end{aligned} \tag{1}$$

where Γ is bounding surface of the computational domain, function G is free space solution to inhomogeneous Helmholtz equation $\nabla^2 G + k^2 G = -\delta$, and α is coefficient ranging from 0 to 1 that needs to be calculated if the observation point is on the bounding surface Γ [6].

For the coupled BEM/FEM formulation it is beneficial to specify the magnetic field entirely in terms of tangential components of electromagnetic fields. Thus, by using the equation $\vec{H} \cdot \vec{n}\,' = -\frac{j}{\omega\mu} \nabla_s \cdot \vec{n}\,' \times \vec{E}$, where $\vec{n}\,'$ is an outward normal to Γ, and by taking the cross product of the equation (1) with outward surface normal $\vec{n}$ it is obtained:

$$\begin{aligned}\alpha\vec{H}_{ext} \times \vec{n} =& \vec{H}_{inc} \times \vec{n} + \\ & \vec{n} \times \frac{j}{\omega\mu} \oint_\Gamma \nabla' G \left(\nabla'_s \cdot \vec{E}_{ext} \times \vec{n}\,'\right) dS' + \\ & - j\omega\epsilon\vec{n} \times \oint_\Gamma d\vec{S}' \times G\vec{E}_{ext} \\ & - \vec{n} \times \oint_\Gamma \left(d\vec{S}' \times \vec{H}_{ext}\right) \times \nabla' G\end{aligned} \tag{2}$$

where ∇'_s is a surface divergence operator and the vectors $\vec{n}$ and $\vec{n}\,'$ are both surface unit normals but at different points on the surface Γ. Although the equation (2) is now expressed as the function of tangential components of electromagnetic fields it is still not specified in terms of interior fields $\vec{E}$ and $\vec{H}$. But, from electromagnetic theory it follows that the tangential components of electromagnetic fields are continuous on surface Γ, hence:

$$\vec{n} \times \vec{E}_{ext} = \vec{n} \times \vec{E}_{ext} \tag{3}$$

$$\vec{n} \times \vec{H}_{ext} = \vec{n} \times \vec{H}_{ext} \tag{4}$$

Substituting the equations (3) and (4) into the equation (2) we obtain the boundary integral formulation for magnetic field specified in terms of tangential components of interior fields $\vec{E}$ and $\vec{H}$:

$$\begin{aligned}\alpha\vec{H} \times \vec{n} =& \vec{H}_{inc} \times \vec{n} + \\ & \vec{n} \times \frac{j}{\omega\mu} \oint_\Gamma \nabla' G \left(\nabla'_s \cdot \vec{E} \times \vec{n}\,'\right) dS' + \\ & - j\omega\epsilon\vec{n} \times \oint_\Gamma d\vec{S}' \times G\vec{E} \\ & - \vec{n} \times \oint_\Gamma \left(d\vec{S}' \times \vec{H}\right) \times \nabla' G\end{aligned} \tag{5}$$

The interior of the computational domain shown in the Fig. 1 is governed by the Helmholtz equation which can be obtained from time-harmonic Maxwell equations as:

$$\nabla \times \left(\frac{j}{\omega\mu} \nabla \times \vec{E}\right) - (\sigma + j\omega\epsilon)\,\vec{E} = 0 \tag{6}$$

When the computational domain is discretized with tetrahedral elements, over a single tetrahedron the interior electric and the magnetic fields are approximated using tangential edge elements:

$$\vec{E} = \sum_j^N \delta_j \vec{W}_j e_j \tag{7}$$

$$\vec{H} = \sum_j^N \delta_j \vec{W}_j h_j \tag{8}$$

where $N = 6$ for tetrahedra and $N = 3$ for triangles on the surface Γ. The functions $\vec{W}_j$ are vector basis functions, the coefficient $\delta_j = \pm 1$, and h_j and e_j are edge element coefficients associated with each edge of the tetrahedron (or triangle). Following the thoroughly described procedure

detailed in [6] the equations (5) and (6) yield the matrix equation shown in the Fig. 2.

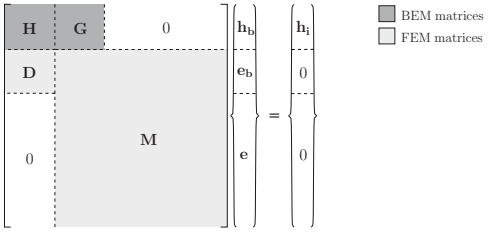

Fig. 2. The BEM-FEM matrix for inhomogeneous scattering problems. Submatrices $\mathbf{H}$ and $\mathbf{G}$ come from the BEM part of the formulation, and submatrices $\mathbf{D}$ and $\mathbf{M}$ come from the FEM part of the formulation. Coefficients h_b and e_b are unknown coefficients at Γ, coefficients e are unknown coefficients inside computational domain and h_i are coefficients computed from incident magnetic field.

The matrix equation in Fig. 2 can be solved for unknown coefficients e and h, and from these coefficients the electric field can be calculated using (7) and (8) everywhere inside the inhomogeneous computational domain.

The presented method for the calculation of interior electric field is well tested over the course of almost a decade and published in series of scientific papers involving the electromagnetic scattering from inhomogeneous targets [6], [11]–[13].

III. The Head Model

The geometry of the head shown in the Fig 1 is obtained from IEEE SAM Model which is commonly used head phantom to benchmark levels of energy delivered by mobile phones to the human head [14]. The entire computational domain is discretized into tetrahedrons using AnSyS ICEM software with restriction that no element size is greater than $\lambda/10$ which is standard restriction for EM scattering problems.

However, without the airbox, the surface of the head represents a highly irregular surface which means many triangles are needed to correctly represent the geometry of the head. For example, our head geometry is discretized into 3,511,924 tetrahedrons which yield 151,185 triangles at the surface of the head. The triangles on the surface of the head yield 257,014 unique edges which translates to 514,029 unknows (257,014 for coefficients e_b and $257,014$ for coefficients h_b). Since matrices $\mathbf{H}$ and $\mathbf{G}$ come from BEM, these are dense matrices, and the required memory storage for storing $257,014 \times 514,029$ complex numbers is approximately $1.968\,\mathrm{TB}$ (terabytes). Any direct matrix solver, Intel Pardiso for example, would require many more terabytes of computer memory in order to solve for vector of unknown coefficients shown in the Fig. 2. On the other hand, matrices $\mathbf{D}$ and $\mathbf{M}$ that come from FEM part of EM scattering problem require minimal storage because they are sparse and symmetric.

This is precisely the reason why we have immersed the human head into the airbox shown in the Fig 1, the surface of which is not irregular. The element size on the surface of airbox is $1\,\mathrm{cm}$ which adheres to the requirement that no element is larger than $\lambda/10$. At the surface of airbox, there is merely 8,984 triangles (shown in the Fig. 4) which yield

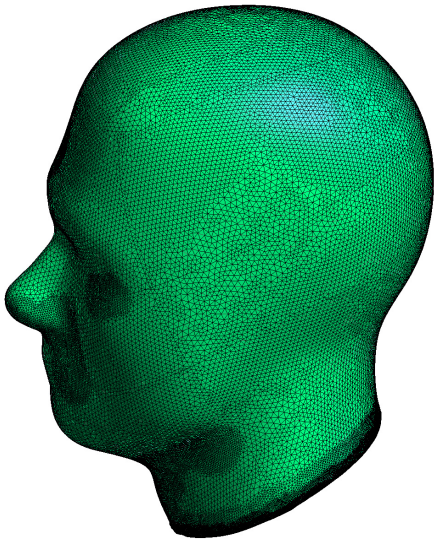

Fig. 3. The surface of the phantom head is represented by 151,185 triangles, and the interior of the head is represented by 3,511,924 tetrahedrons.

13,476 unique edges on the surface of airbox. In this case the storage requirement is 2.7 GB ($13,476 \times 13,476 \times 16$ bytes) for matrix $\mathbf{H}$ and 2.7 GB for matrix $\mathbf{G}$.

Clearly, from the viewpoint of memory storage (and the computational time) it is significantly more advantageous to enclose the head into the airbox, so that surface of airbox represents the boundary surface Γ of the computational domain, than using the surface of the head as the boundary surface of the computational domain.

The final model consists of 7,926,464 tetrahedral elements in total; 3,511,924 tetrahedral elements for head and 4,414,540 tetrahedral elements for airbox. The cross section of tetrahedral model is shown in Fig. 5, and the darker parts around the head represent a large number of very small tetrahedra (due to

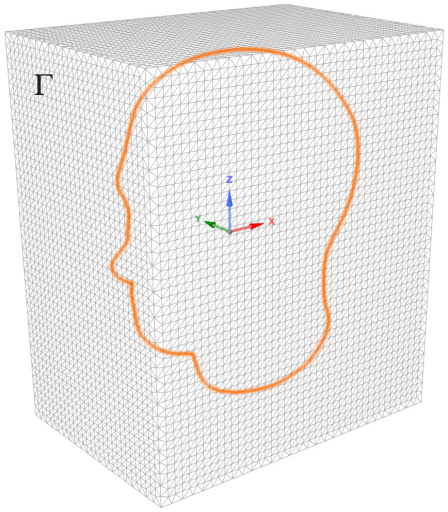

Fig. 4. The surface of the airbox is discretized using only 8,984 triangles yielding 13,476 unique edges, and $2 \times 13,476$ unknown coefficients e_b and h_b at the surface Γ.

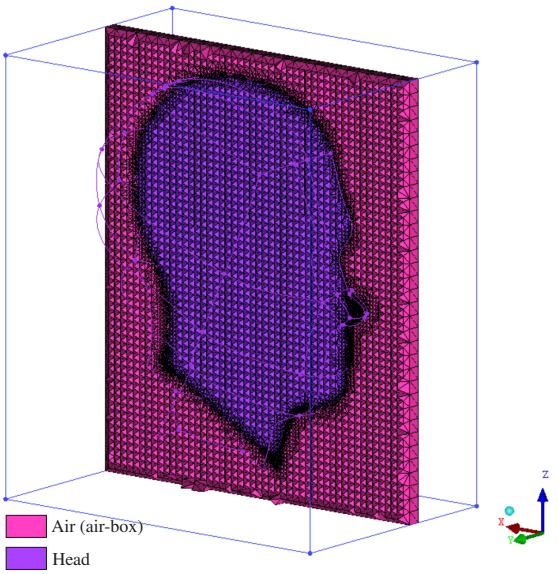

Fig. 5. Cross section of the tetrahedral mesh of the computational domain. The model consists of 7,926,464 tetrahedral elements in total; 3,511,924 tetrahedral elements for head and 4,414,540 tetrahedral elements for airbox.

irregularity of head's surface). Because most of the elements are in the interior of the computational domain, these only contribute to FEM matrices $\mathbf{D}$ and $\mathbf{M}$ which are sparse and symmetric. FEM matrices in hybrid BEM/FEM do not significantly contribute to memory storage nor to computational time required for filling and solving the matrix equation shown in the Fig. 2.

The electrical and thermal properties of the head and the air-box are shown in the Table I. The electrical properties of the head at 2.45 GHz are head tissue properties recommended by IEEE Standard 1528-2013. The blood perfusion W_b, the thermal conductivity λ and the metabolic rate are taken from the ref. [15].

TABLE I
ELECTRICAL AND THERMAL PROPERTIES

Property	Symbol	Units	Head	Air-box
Conductivity	σ	$\frac{\mathrm{S}}{\mathrm{m}}$	1.8	0.0
Relative permittivity	ϵ_r		39.1	1.0
Mass density	ρ	$\frac{\mathrm{kg}}{\mathrm{m}^3}$	1000.0	1.225
Thermal conductivity	λ	$\frac{\mathrm{W}}{\mathrm{mK}}$	0.41	0.03
Blood perfusion	W_b	$\frac{\mathrm{W}}{\mathrm{m}^3\mathrm{K}}$	7443.786	0.0
Metabolic rate	$\dot{Q}_m$	$\frac{\mathrm{W}}{\mathrm{m}^3}$	0.0	0.0

IV. SAR COMPUTATION

From the electric field values obtained using the computational method explained in the section II, the values of SAR can be calculated using the following equation:

$$SAR = \frac{\sigma}{2\rho}\left|\vec{E}\right|^2 \tag{9}$$

Here, we are interested in obtaining the nodal SAR values at vertices of tetrahedrons, and the computed SAR values will be used as an input for thermal rise computation presented in the section V.

From electromagnetic theory it follows that the electric field values are not necessarily continuous across inter-element boundaries which also means that SAR values are also not continuous across elements. Moreover, σ and ρ are not continuous across inter-element boundaries. To obtain the nodal values of SAR at the vertices of tetrahedrons we simply sum the average SAR values of all tetrahedrons sharing the specific vertex and divide by the number of such tetrahedrons:

$$SAR_{v_i} = \frac{\sum_{j=1}^{N} SAR_{avg}^{e_j}}{N} \tag{10}$$

where $SAR_{avg}^{e_j}$ is average SAR calculated for j^{th} tetrahedron, and N is the number of tetrahedrons sharing the vertex v_i. This method of SAR computation was compared to some published results, such as SAR caused by the plane wave impinging on lossy sphere [16], and the results are in good agreement.

V. THERMAL RISE COMPUTATION

Steady state heat transfer in a biological tissue is commonly described by the Pennes bioheat equation. This equation was introduced by Harry H. Pennes in 1948 in his pioneering mathematical work relating the heat transfer and the blood perfusion [17]. Pennes bioheat equation is widely used in applications like electromagnetic dosimetry [12], [13] and hyperthermia treatment [18], [19]. In the form used in electromagnetic dosimetry the Pennes bioheat equation reads:

$$\nabla \cdot (\lambda \nabla T) + W_b c_b (T_a - T) + \dot{Q}_m + \dot{Q}_{em} = 0 \tag{11}$$

where λ is thermal conductivity, c_b is specific heat capacity of blood ($\mathrm{J\,kg^{-1}\,K^{-1}}$), T_a is arterial blood temperature, T is the temperature of the tissue, and $\dot{Q}_m$ is metabolic heat source. The rest of the parameters are specified in the Table I.

While the parameters λ, W_b, c_b, $\dot{Q}_m$ are obtained from the years of measurement and the experimentation on biological tissues [20], [21], the electromagnetic heat source $\dot{Q}_{em}$ at any particular point in space is calculated using the following equation:

$$\dot{Q}_{em} = \rho SAR \tag{12}$$

where ρ is the mass density given in $\left[\mathrm{kg/m^3}\right]$. At the bounding surface of the model we impose the Neumann boundary condition:

$$\lambda \frac{\partial T}{\partial \vec{n}} = \lambda (\vec{n} \cdot \nabla T) = -h_c (T - T_{amb}) \tag{13}$$

where $\vec{n}$ is an outward surface unit normal, T_{amb} is the temperature of the ambient taken as $T_{amb} = 22°\mathrm{C}$, and h_c is convective heat transfer coefficient which describes the rate of heat transfer between a surface of the model and a surrounding fluid. Because the surrounding fluid is still (motionless) air, h_c is taken to be $h_c = 20\mathrm{W/m^2°C}$.

The thermal rise in head induced by EM wave can now be computed using FEM. The FEM formulation is based on weighted residual statement of Galerkin, where the weighing functions are identical to the basis functions. Thus, the FEM formulation is obtained by multiplying the equation (11) by basis functions N_i and integrating over the volume V of the computational domain:

$$\int_V N_i \left[\nabla \cdot (\lambda \nabla T) + W_b c_b (T_a - T) + \dot{Q}_m + \dot{Q}_{em}\right] dV = 0 \tag{14}$$

Assuming λ is a piecewise constant, using the divergence theorem, and using the Neumann boundary condition (13) the weak formulation is obtained:

$$\begin{aligned} &\int_V [\lambda \nabla N_i \cdot \nabla T + N_i W_b c_b T]\, dV + \oint_\Gamma h_c N_i T dS = \\ &\int_V N_i \left[W_b c_b T_a + \dot{Q}_m + \rho SAR\right] dV + \oint_\Gamma h_c T_{amb} N_i dS \end{aligned} \tag{15}$$

Using the standard Galerkin procedure for FEM, and using the expansion $T = \sum_j N_j T_j$, the system of equations is obtained:

$$[A]\{T\} = \{b\} \tag{16}$$

where $\{T\}$ is unknown vector of nodal temperatures and $\{b\}$ is known vector coming from Neumann's boundary condition, SAR computation, known arterial blood temperature and known metabolic heat sources.

VI. Results

The results of EM field computation using methods described in the section II are shown in the Fig. 6 and Fig. 7. In the Fig. 6 the magnitude of electric field is shown on the surface of human head and inside the part of the airbox. The EM wave at frequency $f = 2.45\,\mathrm{GHz}$ has wavelength $\lambda = 12.23\,\mathrm{cm}$ in air. Because inside the human head $\epsilon_r = 39.1$ the wavelength changes, thus $\lambda_h = c/f = 1/\left(\sqrt{\mu\epsilon} f\right) = 1.95\,\mathrm{cm}$. This is clearly visible in the Fig. 7 where the cross section of the magnitude of electric field inside the human head is shown.

Using the computed magnitude of electric field the SAR is computed using the method described in the section IV and it was an input to bio-heat equation solved by methods described in section V. At frequency $f = 2.45\,\mathrm{GHz}$ the penetration depth of electric field is $\delta = 1/\sqrt{\pi f \mu \sigma} \approx 7\,\mathrm{mm}$. For that reason there is not much heating caused by EM waves, as indicated in the Fig. 8. The temperature field shown in Fig. 8 is mainly caused by blood perfusion W_b. However, at bluetooth frequencies there is some temperature increase at the surface of the head phantom, as shown in the Fig. 9.

VII. Conclusion

This paper presented the computation of the temperature rise in IEEE recommended human head phantom caused by incident time-harmonic EM wave at bluetooth frequencies. The computation of thermal rise caused by EM fields is a three step process: one first has to compute the electric field by solving inhomogeneous EM scattering problem, then SAR has to be computed and then Pennes bioheat equation has to be solved to obtain the temperature field. The calculation of EM scattering is particularly computationaly expensive because it combines BEM with FEM, and BEM yields dense matrices. As demonstrated in this paper, this computational cost can be reduced by carefully crafting the computational model. It was also demonstrated that because the penetration depth of EM fields at blueetooth frequencies is not significant the dominant effect of EM heating of head phantom is at the surface of the

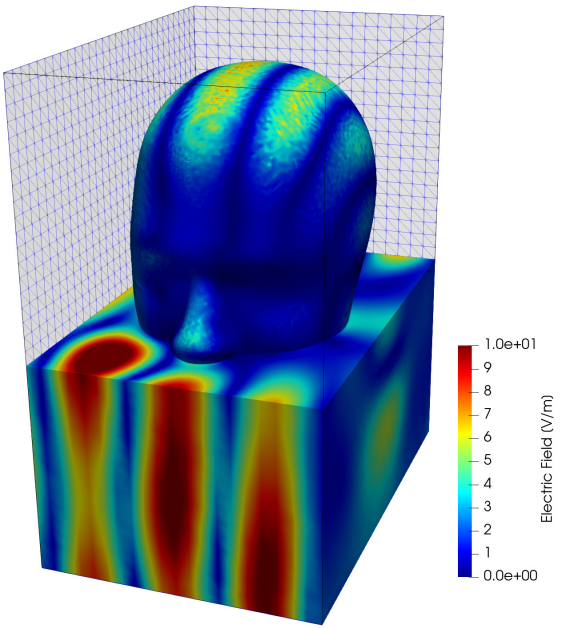

Fig. 6. The magnitude of the induced electric field on the surface of human head phantom and in the surrounding air. The airbox was cut at the nose, and only the lower portion of the airbox is shown.

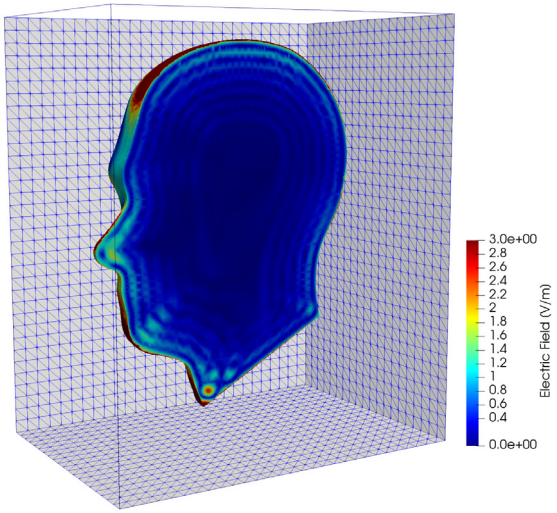

Fig. 7. The magnitude of the induced electric field inside human head phantom. The airbox is not shown. The wavelength of EM waves has shortened because ϵ_r in head is larger than in air.

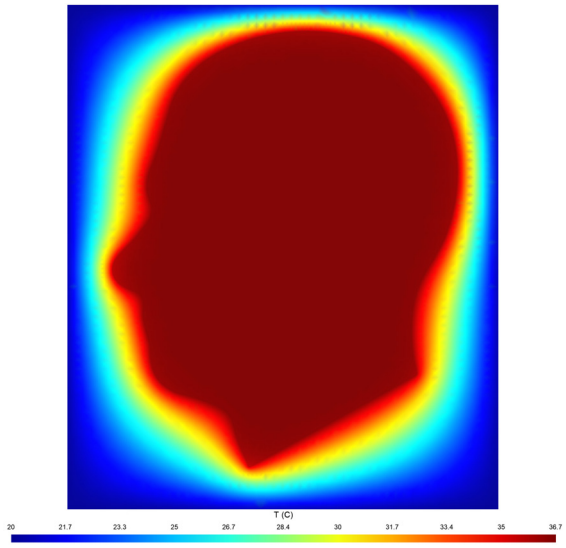

Fig. 8. The cross section of the temperature field in the $x - z$ plane.

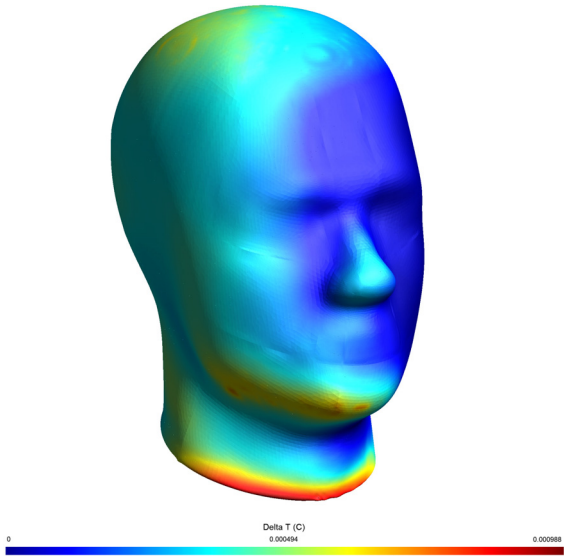

Fig. 9. The temperature increase on the surface of the human head phantom caused by the time harmonic EM fields with power density of $100\,\mathrm{mW/m^2}$.

phantom. The future work aims to confirm these computations by performing real world measurements on real head phantoms as a part of Croatian Science Foundation project HRZZ-IPS-2024-02-7779.

REFERENCES

[1] IEEE, "IEEE Standard for Safety Levels with Respect to Human Exposure to Electric, Magnetic, and Electromagnetic Fields, 0 Hz to 300 GHz, " in *Phys. Rev.*, in *IEEE Std C95.1-2019*, pp. 1–312, 2019. DOI: 10.1109/IEEESTD.2019.8859679.

[2] ICNIRP, "Guidelines for limiting exposure to electromagnetic fields (100 kHz to 300 GHz)," in *Health Phys* ., vol. 118(5), pp. 438–524, 2020. DOI: 10.1097/HP.0000000000001210.

[3] Y. Ren, Q. Huo Liu, Y. P. Chen, "A Hybrid FEM/MoM Method for 3-D Electromagnetic Scattering in Layered Medium," in *IEEE Trans. Antennas Propag.*, vol. 64(8), pp 3487–3495, 2016. DOI: 10.1109/TAP.2016.2575979.

[4] R. W. Xu, L. X. Guo, H. J. He, W. Liu, "A Hybrid FEM/MoM Technique for 3-D Electromagnetic Scattering From a Dielectric Object Above a Conductive Rough Surface," in *IEEE Geosci. Remote Sens. Lett.*, vol. 13(3), pp 314–318, 2016. DOI: 10.1109/LGRS.2015.2508500.

[5] C. H. Ahn, B. S. Jeong, S. Y. Lee, "Efficient vectorial hybrid FE-BE method for electromagnetic scattering problem," in *IEEE Trans. Magn.*, vol. 30(5), pp. 3136–3139, 1994. DOI: 10.1109/20.312602.

[6] H. Dodig, D. Poljak, M. Cvetković, "On the edge element boundary element method/finite element method coupling for time harmonic electromagnetic scattering problems," in *Int. J. Numer. Methods Eng.*, vol. 122(14), pp 3613–3652 2021. DOI: 10.1002/nme.6675.

[7] J. A. Stratton, L.J. Chu, "Diffraction Theory of Electromagnetic Waves," in *Phys. Rev.*, vol. 56, pp 99–107 1939. DOI: 10.1103/PhysRev.56.99.

[8] J. P. Berenger, "A perfectly matched layer for the absorption of electromagnetic waves," in *J. Comput. Phys.*, vol 114(2), pp 185–200 1994. DOI: 10.1006/jcph.1994.1159.

[9] R. Mittra, O. Rahmani, "Absorbing boundary conditions for the direct solution of partial differential equations arising in electromagnetic scattering problems," in *Prog. Electromagn. Res.*, 1990. DOI: 10.1016/B978-0-444-01518-1.50010-9.

[10] A. Boag, R. Mittra, "A numerical absorbing boundary condition for 3D edge-based finite-element analysis of very low-frequency fields," in *Microw. Opt. Technol. Lett.*, vol. 9, pp. 22-27, 1995. DOI: 10.1002/mop.4650090110.

[11] D. Poljak, D. Cavka, H. Dodig, C. Peratta, A. Peratta,"On the use of the boundary element analysis in bioelectromagnetics," in *Eng. Anal. Bound. Elem.*, vol. 49, pp. 2-14, 2014. DOI: 10.1016/j.enganabound.2014.02.008.

[12] M. Cvetković, H. Dodig, D. Poljak, "Temperature increase in the extracted and compound eye models," in *Proc. 25th International Conference on Software, Telecommunications and Computer Networks (SoftCOM)*, Split, Croatia, 2017, pp. 1-6, doi: 10.23919/SOFTCOM.2017.8115589.

[13] A. Šušnjara, H. Dodig, D. Poljak, M. Cvetković, "Stochastic-Deterministic Thermal Dosimetry Below 6 GHz for 5G Mobile Communication Systems," in *IEEE Trans. Electromagn. Compat.*, vol. 64, no. 5, pp. 1667–1679, 2021. DOI: 10.1109/TEMC.2021.3098431

[14] IEEE Recommended Practice for Determining the Peak Spatial-Average Specific Absorption Rate (SAR) in the Human Head from Wireless Communications Devices: Measurement Techniques, IEEE Standard 1528–2003, 2003.

[15] A. Hirata, "Temperature increase in human eyes due to near-field and far-field exposures at 900 MHz, 1.5 GHz, and 1.9 GHz", in *IEEE Trans. Electromagn. Compat.*, vol. 47(1), pp. 68–76, 2005. DOI: 10.1109/TEMC.2004.842113.

[16] J. X. Zhao, H. M. Lu, J.Deng, "Dosimetry and Temperature Evaluations of a 1800 MHz TEM Cell for in Vitro Exposure with Standing Waves," in *Prog. Electromagn. Res.*, vol. 124, pp 487–510, 2012. DOI: 10.2528/PIER11091204.

[17] H. H. Pennes, "Analysis of Tissue and Arterial Blood Temperatures in the Resting Human Forearm ," in *J. Appl. Physiol.*, vol. 1, pp. 93–122, 1948. DOI: 10.1152/jappl.1948.1.2.93.

[18] G. Resende Fatigate, G. Coelho Martins, M. Lobosco, R. Freitas Reis, "Influence of blood-related parameters for hyperthermia-based treatments for cancer," in *J. Comput. Sci.*, vol. 87, 2025. DOI: 10.1016/j.jocs.2025.102556.

[19] T. Drizdal, G. C. van Rhoon, O. Fiser, D. Vrba, N. van Holthe, J. Vrba, M. M. Paulides, "Assessment of the thermal tissue models for the head and neck hyperthermia treatment planning ," in *J. Therm. Biol.*, vol. 115, 2023. DOI: 10.1016/j.jtherbio.2023.103625.

[20] L. Bianchi, F. Caverzan, M. Cremonesi, F. Grilli, P. Saccomandi, "Thermophysical and mechanical properties of biological tissues as a function of temperature: a systematic literature review ," in *J. Therm. Biol.*, vol. 39, no. 1, pp. 297–340, 2021. DOI: 10.1080/02656736.2022.2028908

[21] M. Elia, "Organ and tissue contribution to metabolic rate," in *JM Kinney, HN Tucker, editors. Energy metabolism: tissue determinants and cellular corollaries*, New York: Raven Press. p 61–80, 1992.